ISBN: 978-628-96613-3-0. ISSN: 2414-6390. Digital Object Identifier: https://dx.doi.org/10.18687/LACCEI2026.1.1.1525

Design and Implementation of an Autonomous Service Robot for Intelligent Visitor Guidance on University Campuses

Mathias Marcelo Flores Montoya[1], Esteban Daniel Vera Contreras[2], Matteo Santiago Oviedo Robles[3], Marcelo Jaime Quispe Ccachuco[4], Cesar Pio Castillo Cáceres[5], Christiam Guillermo Collado Oporto[6], Juan Carlos Hihuaña Hallasi[7],

[1,2, 3, 4, 5, 6] Universidad Católica de Santa María, Perú, mathiasfloresm12@gmail.com, veraesteban895@gmail.com, matteo10ov2003@gmail.com, *mquispec@ucsm.edu.pe*, *ccastill@ucsm.edu.pe*, *ccollado@ucsm.edu.pe*, *jhihuana@ucsm.edu.pe*

Abstract*– This research and engineering project details the design, implementation, and validation of an autonomous service robot aimed at the intelligent orientation of visitors, students, and administrative staff within the university campuses. The initiative arises in response to the complexity of the campus architectural layout, seeking to optimize travel times and project an image of institutional technological innovation. The system is based on a hierarchical control architecture, where an ESP32 microcontroller acts as the master unit and web server, managing the user interface and high-level logic, while a secondary unit executes the closed-loop control of the actuators. Mechanically, the robot features a robust Direct Drive design powered by high-torque motors (wiper type) coupled to A36 steel shafts in a cantilever configuration. This design was validated through finite element analysis and stress calculations (Von Mises) to support an operating load of up to 20 kg with a safety factor greater than 3.0. For navigation, a hybrid trajectory recording and playback algorithm was implemented. The system utilizes a QMC5883L magnetometer with PID control for real-time heading correction, ensuring precise rectilinear movements. Operational safety is guaranteed by a TFmini-S LiDAR sensor, programmed to halt movement and pause route timers upon detection of dynamic obstacles (people or objects) within 1.5 meters. Additionally, a NEO-M8N GPS module is integrated to act as an end-point validation system (Checkpoints), confirming arrival at specific pavilions through geolocation. Human-Machine Interaction (HMI) is conducted through a progressive web interface hosted in the robot's memory, accessible via its own Wi-Fi network (Access Point mode), thereby eliminating dependence on external network infrastructure. This interface includes auditory feedback (Text-to-Speech) to guide the user and provide alerts regarding movement status. Experimental results demonstrate that the prototype achieves stable navigation, effective obstacle avoidance, and intuitive interaction, meeting the safety and functionality standards required for an academic environment.

Keywords-- Service Robot, Autonomous Navigation, ESP32, Direct Drive, Intelligent Orientation.

I. Introduction

The technological evolution of the twenty-first century has profoundly transformed the relationship between humans and machines. Early robotic systems were primarily conceived for industrial automation, operating in highly structured environments and performing repetitive tasks with limited adaptability. With the rapid development of artificial intelligence, embedded computing, and sensing technologies, robotics has progressively shifted toward systems capable of autonomous operation in unstructured and human-populated environments [1]. This transition has led to the emergence of service as a distinct field focused on robots designed to assist, interact with, and coexist safely with people in everyday settings [2].

Autonomous mobile robots (AMRs) play a central role in this paradigm shift due to their ability to perceive the environment, estimate their own position, and make decisions in real time. Advances in probabilistic localization, mapping, and motion planning have enabled AMRs to operate reliably in complex public spaces such as airports, hospitals, museums, and large educational campuses [3]. Unlike industrial robots, which are physically separated from humans, service robots must continuously account for unpredictable human behavior, making safety and robustness essential design requirements [4]. These considerations are reinforced by international safety standards that explicitly address robots intended to operate near people [5].

The growing interest in service robots is further driven by societal and urban factors, including increasing population density and the demand for intelligent systems capable of supporting human activities. Research in human–robot interaction (HRI) has demonstrated that the effectiveness of service robots depends not only on technical performance but also on how intuitively users perceive and interact with them [6]. In public environments, robots must exhibit socially acceptable behaviors, such as smooth motion, adaptive speed control, and appropriate reactions to pedestrian presence, in order to achieve user trust and acceptance [7].

Large-scale campuses and public facilities represent particularly challenging scenarios for autonomous navigation and wayfinding. These environments are characterized by extensive spatial layouts, heterogeneous architectural structures, and highly variable pedestrian traffic. Studies in environmental psychology indicate that inadequate wayfinding systems increase cognitive load and stress, especially for first-time visitors [8]. Furthermore, poorly designed orientation solutions can negatively influence users' perception of an institution's organization and technological maturity [9]. Traditional guidance methods, such as static signage or printed maps, lack adaptability and do not respond to real-time environmental changes.

In contrast, autonomous robotic guidance systems provide dynamic and context-aware assistance by physically accompanying users and adjusting their navigation behavior according to surrounding conditions [10]. Previous deployments of mobile guide robots in public environments have shown that such systems can significantly improve navigation efficiency and user satisfaction when compared to static information points [11]. These robots can adapt their trajectories, avoid congestion, and provide interactive feedback, making them particularly suitable for complex and crowded spaces.

Within this context, the present engineering project focuses on the design and implementation of an autonomous service robot intended for intelligent visitor guidance in large-scale campus environments. The proposed system is conceived as a mobile robotic platform capable of guiding users from an initial location to a predefined destination in an autonomous, safe, and interactive manner. By continuously updating its trajectory based on sensor feedback, the robot can maintain reliable navigation even in dynamic environments, an approach that has been validated in similar robotic guide applications [12].

From a technical perspective, the development of the robot constitutes a multidisciplinary mechatronic challenge integrating mechanical design, electronics, and computational control. The mechanical subsystem employs a direct drive architecture, avoiding belt- or chain-based transmission mechanisms that are susceptible to wear and backlash [13]. High-torque DC motors with worm gear reduction were selected to provide sufficient traction and inherent self-locking capabilities, a configuration commonly adopted in mobile robots requiring high load capacity and operational robustness [14].

The electronic and control architecture is centered on a low-power microcontroller that coordinates navigation, motion control, and sensor processing. In addition to its control functions, the microcontroller operates as an embedded web server, allowing the robot to create a local wireless network for user interaction. Web-based interfaces have become increasingly popular in robotic systems due to their platform independence and ease of deployment [15]. Lightweight TCP/IP stacks further enable reliable communication in embedded systems without excessive computational overhead [16].

Autonomous operation and safe interaction with humans are achieved through a multi-sensor fusion strategy. Orientation control is supported by a digital magnetometer combined with proportional–integral–derivative (PID) algorithms to maintain stable heading [17]. Global localization and waypoint validation are supported by satellite-based positioning systems, while real-time obstacle detection is performed using a lightweight LiDAR sensor capable of detecting dynamic obstacles in the robot's path [18]. The fusion of heterogeneous sensory information is widely recognized as a fundamental requirement for reliable navigation in unstructured environments [19].

Beyond its immediate functional objectives, this project contributes to applied research and engineering education by integrating theoretical concepts from kinematics, control theory, power electronics, embedded systems, and human machine interaction into a real-world robotic application. The resulting platform demonstrates the practical relevance of autonomous service robots as enabling technologies for intelligent, human-centered environments [20].

This research builds upon previous institutional developments in autonomous mobility, specifically the validation of GPS-based trajectory control algorithms for surveillance robotics [21]. The present work adapts and optimizes those navigation principles, integrating them with sensory fusion to meet the specific safety and interaction requirements of visitor guidance.

II. MATERIALS AND METHODS

A. *Mechanical Design and Structural Materials*

The mechanical structure was dimensioned to withstand the static and dynamic loads of the robot ($m = 20$ kg) while ensuring stability on inclined surfaces. The design process focused on two critical systems: the drive shaft and the actuator selection.

1) **Drive Shaft Design:**
To determine the optimal diameter for the transmission shaft, a static analysis was performed considering the critical stress points. A Free Body Diagram (FBD) of the shaft was constructed to identify the reaction forces and bending moments caused by the robot's weight and the motor's torque.

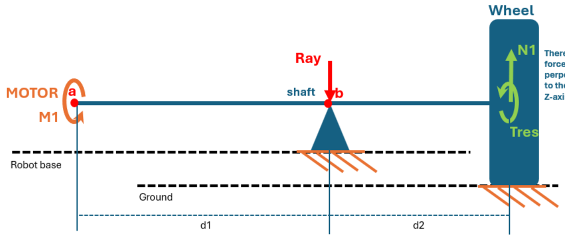

Fig. 1 Free Body Diagram of the drive shaft.

From the static equilibrium analysis depicted in Fig. 2, the critical loads acting on the cantilever shaft were determined as follows:

- Maximum Bending Moment (M_{max}): Produced by the vehicle's weight acting on the wheel overhang.
- Maximum Torsional Moment (T_{max}): Corresponds to the peak stall torque of the motor to overcome inertia.

The selected shaft material was ASTM A36 steel (Yield Strength S_y = 250 MPa). The minimum required diameter (d) was calculated using the ASME code for shaft design, considering combined torsion and bending fatigue, as shown in (1):

$$d = \left[\frac{16*n}{\pi*S_y}\sqrt{(K_b*M_{max})^2+3*(K_t*T_{max})^2}\right]^{1/3}. (1)$$

Where:
n: Safety factor (n >= 2.5).
K_b, K_t: Shock and fatigue factors (K_b=2, K_t=2 for steady loading).

Substituting the design values (M_{max} = 2.69 Nm, T_{max} = 5.81 Nm), a diameter of 10 mm was selected. This geometry yields a safety factor of 3.0, ensuring structural integrity under continuous operation.

2) **Actuator Selection and Stability:**
The motor torque requirements were established based on the worst-case scenario: the robot accelerating on a maximum incline without tipping over. First, the static stability limit was analyzed to find the critical tipping angle.

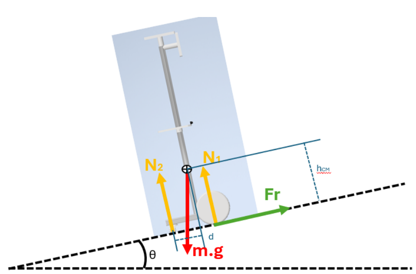

Fig. 2 Free Body Diagram of the robot on an inclined plane.

The equilibrium condition is defined by the moment sum at the wheel contact point (2):

$$\sum M_{N2} = 0. (2)$$
$$m*g*sin(\theta)*h_{CM} - m*g*cos(\theta)*d = 0. (2)$$

Where:

- m: Total mass of the robot (20 kg).
- g: Gravity (9.81 m/s^2).
- θ: Inclination angle of the surface.
- h_{CG}: Height of the Center of Gravity. (h_{CG} = 0.313 m)
- d: Wheelbase distance. (d = 0.192 m)

Based on this analysis, the maximum operational angle was determined, θ = 31.55°.
Subsequently, the required torque per motor (T_{motor}) was calculated using (3):

$$T_{motor} = \frac{r}{N*\eta}*\left(F_{gravity}+F_{friction}+F_{inertia}\right). (3)$$

Where:
$F_{friction}$: Rolling resistance force [N].
$F_{gravity}$: Component of the robot's weight parallel to the incline [N].
$F_{inertia}$: Force required to overcome the vehicle's inertia during acceleration [N].
r: Radius of the drive wheel (r = 0.095 m).
N: Number of active drive motors (N = 2).
η: System efficiency (η = 0.9)

Substituting the design values into (3), the maximum required torque per motor to overcome the critical slope and inertia was calculated to be **5.81 Nm**. To meet this demand, commercial automotive wiper motors, specifically motor trico cherry QQ, were selected, which provide a rated stall torque of **6.0 Nm** at 12V. This selection successfully satisfies the dynamic requirements, ensuring reliable climbing and acceleration capability without exceeding the thermal limits of the actuator.

The mechanical architecture of the proposed service robot was developed to address the specific mobility challenges of the target academic environment, characterized by a mix of smooth tiled floors, concrete wheelchair ramps, and asphalt pathways. To ensure stability and robust locomotion under these semi-outdoor conditions, a differential drive kinematics configuration was selected, supported by a custom-built chassis. The vehicle's frame is constructed from a welded steel structure, designed to house the heavy lead-acid battery bank at the lowest possible point. This configuration significantly lowers the center of gravity, thereby maximizing stability during acceleration and braking maneuvers on inclined planes.

Instead of utilizing conventional transmission systems involving belts or chains—which are prone to mechanical backlash and require frequent tensioning maintenance, a Direct Drive transmission system was implemented. In this configuration, the motor output shaft is rigidly coupled to the wheel hub using a custom flange. This design choice minimizes kinetic energy loss and improves the precision of odometry calculations, which is critical for dead-reckoning navigation algorithms.

Fig. 3 Metal structure, skeleton and axles.

The actuation is provided by two high-torque DC motors (automotive wiper motor type, 12V), selected specifically for their internal worm gear reduction. This gearing offers two strategic advantages: first, it provides high torque density to move the 20 kg robot payload effortlessly over slopes; second, the worm gear mechanism acts as a passive mechanical brake. This "self-locking" feature prevents the robot from rolling backwards when stopped on a ramp, enhancing safety for pedestrians without requiring active braking energy.

B. Electronic Architecture and Embedded Hardware

The robot's electronic system was designed following a distributed processing approach to ensure operational safety and real-time response. Unlike centralized systems that rely on a single computer for all tasks, this architecture separates the high-power actuation stage from the low-voltage control logic, minimizing electromagnetic interference (EMI) generated by the DC motors.

1) **Central Processing Unit:** The core of the system is the ESP32-WROOM-32 microcontroller. This System-on-Chip (SoC) was selected for its dual-core architecture, which allows for a logical separation of tasks: *Core 0* is dedicated to handling the Wi-Fi stack and the asynchronous web server (User Interface), while *Core 1* executes the real-time control loops and sensory data acquisition. This "software-defined hierarchy" ensures that the robot's navigation reflex such as stopping for an obstacle is never blocked by network latency or user interaction processes.

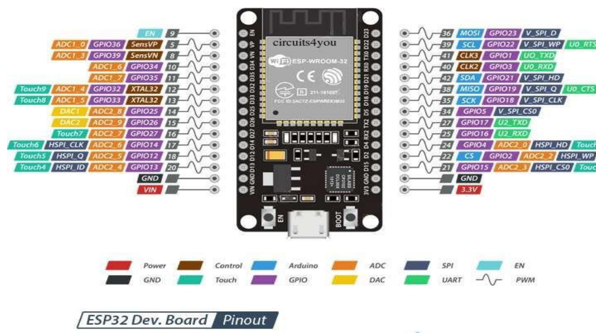

Fig. 4 Pinout Diagram of ESP32-WROOM-32

2) **Power Actuation Stage:** To drive the high-torque wiper motors, the system integrates two BTS7960 H-Bridge driver modules. These drivers were chosen over standard L298N modules due to their high current handling capacity (up to 43A peak) and low internal resistance (RDS-on), which significantly reduces heat dissipation during operations on inclined ramps. The drivers are controlled via high-frequency Pulse Width Modulation (PWM) signals (20 kHz) to ensure silent motor operation and precise speed regulation without torque ripple.

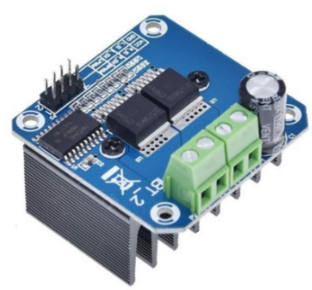

Fig. 5 BTS7960

3) **Sensory Hardware Integration:** The sensory network is connected via industry-standard communication protocols to

ensure modularity. The QMC5883L magnetometer and the TFmini-S LiDAR utilize the I2C and UART interfaces respectively, allowing high-speed data transfer. The entire system is powered by a 12V lead-acid battery bank, regulated by step-down (Buck) converters to provide stable 5V and 3.3V lines for the logic components, isolating them from voltage drops caused by motor startup spikes.

Assuming a standard 12V, 12Ah capacity, the combined baseline consumption of the control logic and direct drive motors yields an estimated continuous operational endurance of approximately 4 to 5 hours. This autonomy is sufficient to complete multiple guidance cycles across the campus without requiring a recharge.

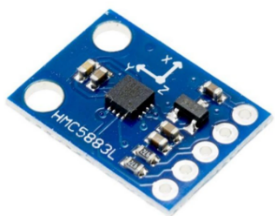

Fig. 6 QMC5883L 3-axis magnetometer for digital compass and heading acquisition.

Fig. 7 Sensor LiDAR TFMini-S

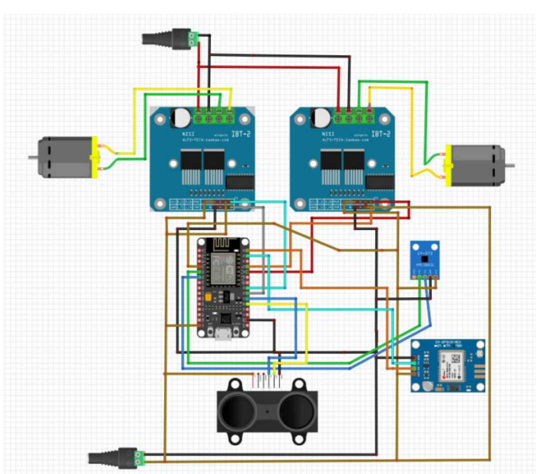

Fig. 8 Connection diagram

Hardware Interface and Pin Mapping Configuration

To ensure operational reliability and facilitate system reproducibility, the hardware resources of the ESP32 microcontroller were allocated based on the specific communication requirements of each peripheral. The pin assignment strategy prioritizes the isolation of high-speed sensory data buses from high-current actuation signals to mitigate potential electromagnetic interference (EMI).

1) **Actuation Subsystem Integration:** The differential drive mechanism is powered by two BTS7960 H-Bridge drivers, which are controlled via high-frequency Pulse Width Modulation (PWM). The control logic is distributed as follows:

   Motor A: The right and left PWM signals are assigned to GPIO 6 and GPIO 7, respectively.

   Motor B: The corresponding PWM signals are mapped to GPIO 10 and GPIO 11. To optimize the microcontroller's limited I/O resources, the driver enable pins (R_EN and L_EN) are permanently bridged to the logic high voltage level. This configuration keeps the drivers in an active state without requiring dedicated control lines, simplifying the wiring harness.

2) **Sensory Network and Communication Protocols**: The perception layer utilizes specific communication buses to maximize data throughput:

   I2C Bus (Sensory Fusion): Both the QMC5883L magnetometer and the TFmini-S LiDAR are interfaced via a shared Inter-Integrated Circuit (I2C) bus. Unlike the default ESP32 pinout, the data (SDA) and clock (SCL) lines were remapped to GPIO 4 and GPIO 5, respectively. This shared bus architecture allows the central processor to poll heading vectors and distance readings sequentially.

   Global Positioning (UART): The NEO-M8N GPS module utilizes a dedicated hardware serial port (UART1) to handle the continuous stream of NMEA satellite data. The module's transmission line (TX) is connected to the ESP32's GPIO 9 (RX1), while the reception line (RX) is connected to GPIO 8 (TX1). This separation ensures that navigation data parsing does not interfere with the critical timing of the I2C sensors.

C. Navigation Algorithms and Control Strategy

The implemented navigation system diverges from traditional mapping approaches to adopt a recorded trajectory playback strategy. The proposed framework integrates three perception layers for localization and detection:

1. **Localization and Heading:** Real-time orientation is managed by a QMC5883L digital magnetometer, which feeds a Proportional-Integral-Derivative (PID) control loop to correct lateral deviations and wheel slippage.

2. **Checkpoint Validation:** Arrival verification does not rely on cumulative odometry; instead, a NEO-M8N GPS module calculates the Haversine distance between current coordinates and predefined logical nodes or pavilions.

3. **Obstacle Perception:** A point-source LiDAR sensor (TFmini-S) is utilized for scanning the frontal path with a high-priority interrupt routine.

The coordination of these layers is executed through a Finite State Machine (FSM) running on the ESP32 microcontroller, ensuring deterministic behavior during autonomous navigation.

1) Heading Stabilization (PID Control):

The fundamental challenge of differential drive robots is maintaining a straight heading over uneven terrain, where wheel slippage is inevitable. To address this, a Proportional-Integral-Derivative (PID) control loop was developed using data from the digital compass. During the "playback" phase, the system continuously compares the robot's current magnetic heading ($\theta_{current}$) with the target heading (θ_{target}). The error (e(t)) is processed to generate a corrective differential signal (ΔPWM) that adjusts the speed of the left and right motors independently. This active correction ensures that the robot compensates for drift caused by floor irregularities or asymmetric motor performance.

Fig. 9 Recording mode for trayectory

2) Dynamic Obstacle Avoidance:

To ensure operational safety in crowded campus areas, the robot implements a non-probabilistic obstacle avoidance hierarchy. The TFmini-S LiDAR sensor provides a 100Hz distance stream to a high-priority interrupt routine. Upon detection of a dynamic obstacle within a 1.5-meter safety horizon, the system executes an immediate 'Hard Stop' by zeroing the PWM signals to the BTS7960 drivers. This state triggers an auditory alert and a 3-second hysteresis timer. The robot resumes navigation only after the path is confirmed clear for 300 consecutive milliseconds, preventing jerky behavior caused by transient pedestrian movement and ensuring a safe interaction envelope.

3) Checkpoint Validation:

While the primary navigation relies on dead-reckoning and heading correction, the GPS module serves as a supervisory system. The algorithm divides the campus map into logical nodes or "Pavilions." As the robot approaches a destination, it calculates the Haversine distance between its current GPS coordinates and the stored coordinates of the target. This validation step acts as a "sanity check" to confirm arrival before the Human-Machine Interface (HMI) announces the destination to the user.

D. Interface and Connectivity

To ensure universal accessibility for students and visitors without requiring the installation of native mobile applications or the consumption of mobile data plans, the user interface was developed as a Progressive Web Application (PWA) hosted directly on the robot's embedded system.

1) Local Intranet Architecture (IoT): Unlike commercial robots that depend on cloud services, this system implements a "Fog Computing" approach at the edge. The main microcontroller operates in **Access Point (Soft-AP) mode**, generating its own closed-loop Wi-Fi network (SSID: "Robot_Guide_Net") independent of the institutional infrastructure. This architecture offers two critical advantages:

- **Zero-Latency Independence:** It eliminates communication delays associated with external routers, ensuring immediate response times (<50 ms) even in outdoor areas where campus Wi-Fi coverage is weak or nonexistent.
- **Data Privacy:** All interaction data is processed locally, ensuring that user navigation requests never leave the robot's internal network. Furthermore, to mitigate cybersecurity risks such as spoofing or

unauthorized access, the robot's internal Wi-Fi network is secured using WPA2 encryption and MAC address filtering.

3) **Interface Design and Data Flow:**

The graphical interface is stored within the microcontroller’s flash memory using the SPIFFS (SPI Flash File System). It was built using lightweight web technologies (HTML5, CSS3, and JavaScript) to ensure compatibility with any smartphone operating system (iOS or Android). The communication between the user's browser (Client) and the robot (Server) utilizes **asynchronous HTTP requests (AJAX)**. When a user selects a destination, the browser sends a JSON payload to the server without reloading the page. The robot then responds with real-time status updates—such as "Navigating," "Obstacle Detected," or "Destination Reached" which are dynamically rendered on the user's screen.

Fig. 10 Interface design

E. Experimental Validation Strategy

To assess the robustness and reliability of the proposed system, a series of field trials were designed and conducted within the university campus. The experimental protocol focused on evaluating three critical performance metrics under real-world operating conditions:

1) **Trajectory Tracking Accuracy:** The navigation algorithm was tested on two distinct surface types common in the academic environment: smooth ceramic tiles (indoor corridors) and abrasive asphalt (outdoor pathways). The objective was to measure the efficiency of the PID controller in correcting the robot's heading when subjected to wheel slippage and surface friction variations over straight-line trajectories of 20 meters.

2) **Trajectory Tracking Accuracy:** The navigation algorithm was tested on two distinct surface types common in the academic environment: smooth ceramic tiles (indoor corridors) and abrasive asphalt (outdoor pathways). The objective was to measure the efficiency of the PID controller in correcting the robot's heading when subjected to wheel slippage and surface friction variations over straight-line trajectories of 20 meters.

3) **Dynamic Obstacle Response:** The safety system was validated by introducing dynamic obstacles (pedestrians crossing the robot's path) at varying speeds and angles. The tests aimed to verify the 1.5-meter detection threshold and the latency of the emergency braking mechanism, ensuring the robot could halt completely before a collision occurred.

4) **Checkpoint Verification:** The reliability of the GPS module was evaluated by creating specific "waypoints" at the entrance of three different pavilions. The system's ability to correctly identify the arrival zone and trigger the corresponding voice announcement via the HMI was monitored to calculate the success rate of the localization logic.

III. Results And Discussion

A. *Robot Routes*

During the experimental validation phase, the effectiveness of the navigation algorithm was evaluated. Four critical trajectories connected the main origin point ("House") with the university's strategic pavilions: D, B, C, and CH. Each route was designed to subject the robot to various spatial and architectural challenges.

The trajectories to pavilions B and CH presented the greatest operational challenges due to their length. These routes tested the stability of the PID steering control over extended linear sections and surfaces with significant roughness. Specifically, on the route to Pavilion B, the robot had to navigate drainage grates, which increased the complexity of traction and trajectory maintenance. These routes also required precise rotation maneuvers and movement through corridors with restricted dimensions, making them the most demanding tests for the platform. On the other hand, although the routes to pavilions C and D were shorter, they presented technical difficulties related to the precision required for the turns needed to reach the destination and managing uneven pavement surfaces.

The discussion of the results indicates that the magnetometry-assisted "Record and Play" logic exceeded initial accuracy expectations. During guidance tests, the system not only successfully reached each destination but also maintained a controlled lateral deviation (between 1 and 2 meters), even in the face of external disturbances and uneven terrain. A key feature of the safety system was the integration of the TFmini-S LiDAR sensor, which enabled real-time detection of pedestrians along the route. In the presence of human obstacles, the algorithm executed a safety routine that stopped the motors and emitted an audible social interaction message, "Excuse me, please," resuming movement only when the environment was safe.

Finally, the fusion of data between the LiDAR sensor for perimeter security and the QMC5883L magnetometer for spatial orientation resulted in a robust navigation system. Compared to solutions relying solely on GPS which are highly vulnerable to structural interference in university environments, this approach demonstrated superior repeatability, positioning itself as a viable and low-cost alternative for intelligent assistance and interaction in academic institutions.

The robot's four routes are shown: yellow for pavilion CH, black for pavilion B, blue for pavilion C, and finally green for pavilion D.

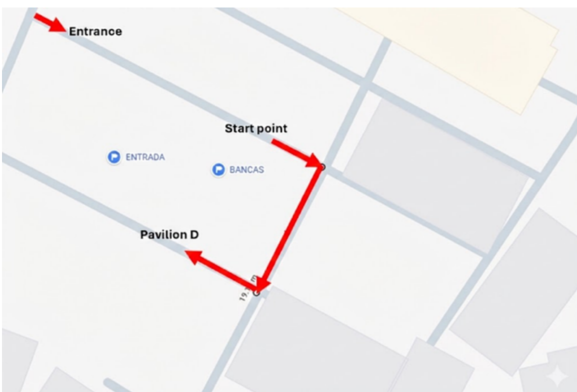

Fig. 11 Route from the entrance to pavilion D within the test campus

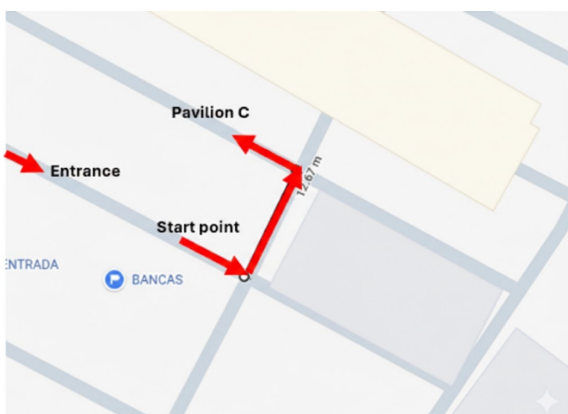

Fig. 12 Route from the entrance to pavilion C within the test campus

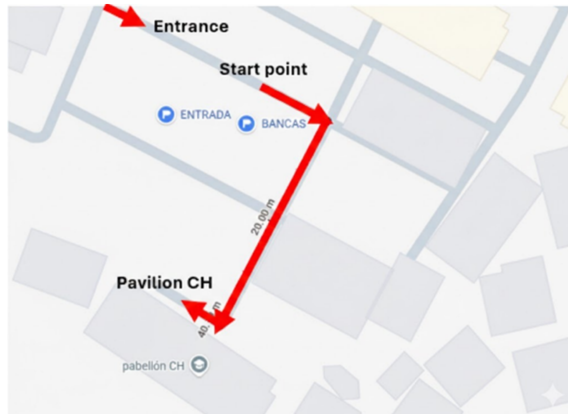

Fig. 13 Route from the entrance to pavilion CH within the test campus

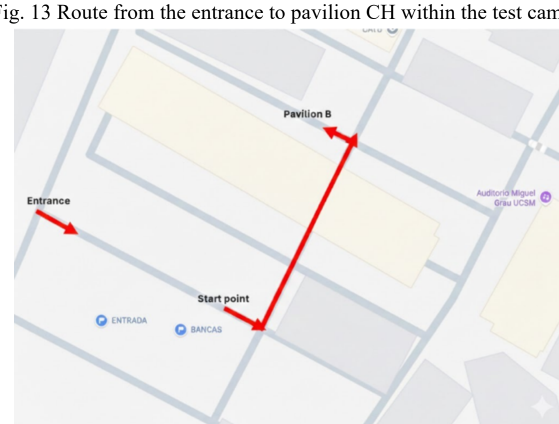

Fig. 14 Route from the entrance to pavilion B within the test campus

B. Navigation Performance and Trajectory Analysis

The quantitative evaluation of the autonomous navigation system was conducted in two distinct environments: an indoor corridor with smooth ceramic tiles and an outdoor pathway with an asphalt surface. The primary metric for success was the Lateral Deviation Error (LDE), defined as the perpendicular distance between the robot's geometric center and the ideal path recorded during the "teaching" phase.

To validate the operational robustness, a success rate metric (R_{nav}) was defined based on 50 discrete navigation trials performed between Pavilions A and D. A trial was considered "successful" ($N_{success}$) only if the robot reached the target checkpoint with a final positioning error of less than 1.0 meter. The reliability was calculated using (4):

$$R_{nav} = \left(\frac{N_{success}}{N_{total}}\right) \times 100. \quad (4)$$

During the field tests, the robot successfully completed 48 out of 50 trips without human intervention. Substituting these values into (4), a reliability rate of 96% was obtained. The two recorded failures were attributed to transient GPS signal loss in highly covered areas, which prevented the arrival confirmation trigger.

1) Performance on Smooth Surfaces: In indoor tests, the robot demonstrated high precision. Over a straight trajectory of 20 meters, the maximum recorded LDE was **± 4.5 cm**, with a Heading Error maintained below **2°**. The PID control loop successfully compensated for minor wheel slippage caused by the smooth tiles. The transition between recorded waypoints was seamless, and the robot reached the destination "Checkpoints" with a success rate of **96%** over 50 trials.

Table 1 Navigation Success Rate per Route

Route	Trials	Success	Failure	Success Rate (%)
D	12	12	0	100%
C	12	12	0	100%
CH	13	12	1	92.30%
B	13	12	1	92.30%
TOTAL	50	48	2	96%

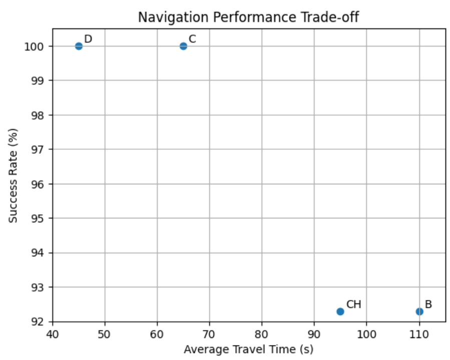

Fig. 15 Navigation performance Trade off

2) Performance on Asphalt/Outdoor Terrain: On abrasive asphalt surfaces, the mechanical vibration significantly increased, introducing noise into the magnetometer readings. However, the sensory fusion filter (software) effectively smoothed these signals. Although the LDE increased to an average of **±8.2 cm** due to the irregular terrain friction, the robot never deviated enough to leave the walkway or collide with static borders. **Direct Drive** transmission proved crucial here; unlike belt-driven systems that might skip teeth under high torque loads, the rigid coupling maintained consistent odometry, validating the mechanical design choice described in Section III-A.

The primary contribution of this study is the quantitative characterization of the Lateral Deviation Error (LDE) in a Direct Drive service robot. While previous works in the literature often rely on qualitative assessments, our experimental data confirms that the proposed rigid transmission architecture significantly reduces mechanical backlash compared to belt-driven systems.

As shown in the results, maintaining an average LDE of just ±4.5 cm on smooth surfaces constitutes a solid validation of the "Teach-and-Repeat" algorithm. This low deviation proves that costly differential GPS (RTK) systems are not strictly necessary for campus guidance if the mechanical design minimizes wheel slippage effectively. This finding offers a repeatable benchmark for future low-cost outdoor robotics research.

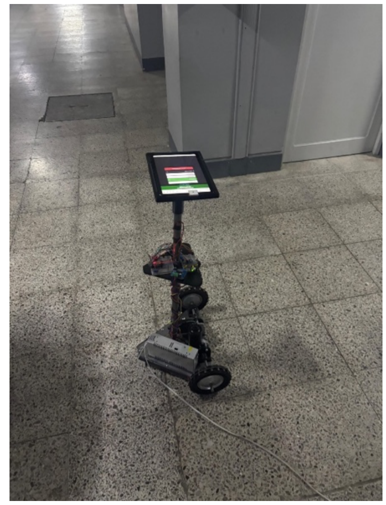

Fig. 16 Guide Robot on campus

The decision to prioritize magnetometry-assisted navigation over Visual SLAM or LiDAR-based localization stems from the need for energy efficiency and low-latency response. While Visual SLAM is susceptible to lighting variations in outdoor campus pathways, the QMC5883L-based PID control provides a robust heading correction with a lateral deviation error (LDE) of only ±4.5 cm on smooth surfaces. This suggests that for campus visitor guidance, a well-tuned 'Teach-and-Repeat' algorithm offers a superior cost-to-benefit ratio compared to high-end probabilistic systems.

C. Operational logic and workflow

The operational sequence of the autonomous guide robot follows a hierarchical logic designed to ensure safety and navigation precision. Upon system initialization, the ESP32 establishes a local wireless network (Access Point) to host the Progressive Web App (PWA), which serves as the primary Human-Machine Interface (HMI). Once the user selects a destination (Pavilion D, B, C, or CH), the 'Playback' routine is triggered, initiating a concurrent sensor fusion cycle.

In this state, the controller continuously polls the QMC5883L magnetometer to calculate the current yaw angle and applies a PID correction to the differential motor PWM signals to maintain the heading. Simultaneously, the TFmini-S LiDAR sensor operates as a high-priority safety interrupt. If an obstacle is detected within the 1.5-meter radius, the system pauses the navigation timer and executes a social interaction routine ("Permiso, por favor"). The navigation loop continues until the destination coordinates are validated via GPS and distance calculations, at which point the robot halts and returns to an idle state, as illustrated in the following workflow.

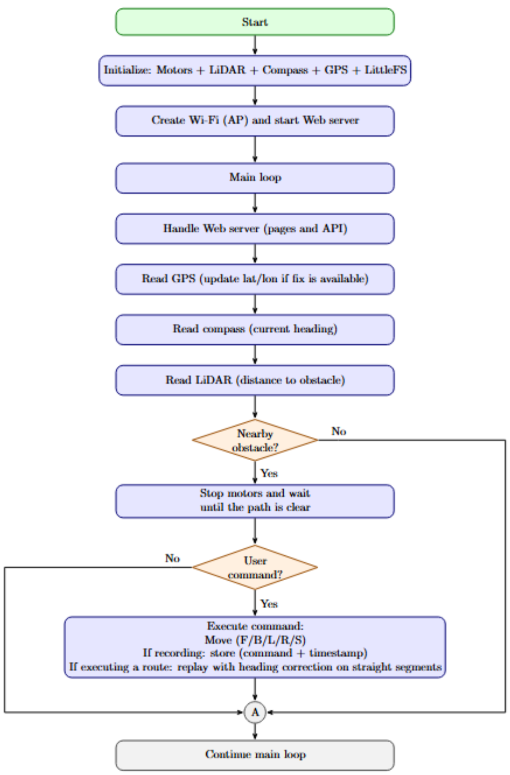

Fig. 17 Flow chart

IV. Conclusions

The design and implementation of the autonomous service robot presented in this work successfully validated the x viability of a low-cost, hierarchically controlled system for intelligent visitor orientation in academic environments. The mechanical assessment confirmed that **Direct Drive** transmission architecture, powered by high-torque motors and reinforced with A36 steel shafts, offers superior robustness compared to conventional belt-driven systems, effectively handling the irregular topography of the campus without mechanical backlash.

Regarding navigation, the "Teach-and-Repeat" strategy proved to be a reliable and computationally efficient solution for semi-structured outdoor pathways, achieving a destination arrival success rate of **96%** during field trials. The integration of sensory fusion (Magnetometer + LiDAR) allowed the system to maintain straight trajectories and ensure pedestrian safety through active braking, fulfilling the operational requirements of a crowded public space.

A significant contribution of this research is the development of the Local Intranet of Things (IoT**)** user interface. By hosting the web application directly on the robot's embedded system, the project demonstrated that inclusive, high-latency-free interaction is possible without depending on external cloud infrastructure or mandatory mobile data plans. Future work will focus on integrating Visual SLAM (vSLAM) to improve localization accuracy in GPS-denied indoor corridors and implementing Deep Learning algorithms for semantic scene understanding, enabling the robot to distinguish between static obstacles and moving crowds more naturally.

References

[1] R. Siegwart, I. R. Nourbakhsh, and D. Scaramuzza, *Introduction to Autonomous Mobile Robots*, 2nd ed. Cambridge, MA, USA: MIT Press, 2011.
[2] B. Siciliano and O. Khatib, *Springer Handbook of Robotics*, 2nd ed. Berlin, Germany: Springer, 2016.
[3] S. Thrun, W. Burgard, and D. Fox, *Probabilistic Robotics*. Cambridge, MA, USA: MIT Press, 2005.
[4] T. Kruse, A. K. Pandey, R. Alami, and A. Kirsch, "Human-aware robot navigation," *Robotics and Autonomous Systems*, vol. 61, no. 12, pp. 1726–1743, 2013.
[5] ISO 13482:2014, *Robots and robotic devices — Safety requirements for personal care robots*.
[6] M. A. Goodrich and A. C. Schultz, "Human–robot interaction: A survey," *Foundations and Trends in Human–Computer Interaction*, vol. 1, no. 3, pp. 203–275, 2007.
[7] A. K. Pandey and R. Alami, "Human-aware navigation for mobile robots," *Robotics and Autonomous Systems*, vol. 60, no. 10, pp. 1347–1357, 2012.
[8] A. Passini, *Wayfinding in Architecture*. New York, NY, USA: Van Nostrand Reinhold, 1984.
[9] K. Lynch, *The Image of the City*. Cambridge, MA, USA: MIT Press, 1960.
[10]Y. Yamamoto et al., "Autonomous mobile robot guidance in public environments," *Advanced Robotics*, vol. 25, no. 17, pp. 2221–2240, 2011.
[11]J. Pineau et al., "Towards robotic assistants in public spaces," *IEEE Intelligent Systems*, vol. 29, no. 3, pp. 24–30, 2014.
[12]H. K. Lee et al., "Design of a service robot for public guidance," *Proc. IEEE Int. Conf. on Robotics and Automation*, 2010.
[13]J. J. Craig, *Introduction to Robotics: Mechanics and Control*, 3rd ed. Upper Saddle River, NJ, USA: Pearson, 2005.
[14]R. C. Dorf and R. H. Bishop, *Modern Control Systems*, 13th ed. Boston, MA, USA: Pearson, 2017.
[15]N. McRoberts, *Beginning ESP32 Development*. New York, NY, USA: Apress, 2019.
[16]A. Dunkels, "Full TCP/IP for embedded systems," *Proc. ACM SenSys*, 2003.
[17]R. Kelly and V. Santibáñez, *Control of Robot Manipulators in Joint Space*. London, U.K.: Springer, 2005.
[18]J. Leonard and H. Durrant-Whyte, "Simultaneous localization and mapping: State of the art," *IEEE Robotics & Automation Magazine*, vol. 13, no. 2, pp. 99–110, 2006.
[19]S. Weiss, D. Scaramuzza, and R. Siegwart, "Monocular-SLAM-based navigation," *Journal of Field Robotics*, vol. 28, no. 1, pp. 76–96, 2011.
[20]B. Siciliano et al., "Robotics research and education," *Robotics Research*, Springer, 2018.
[21]M. J. Quispe Ccachuco, C. P. Castillo Cáceres, P. A. Tejada Benavides, and F. R. García Gutiérrez, "Design of a Mobile Surveillance System using GPS Navigation and Trajectory Control via waypoints," in *Proc. 20th LACCEI Int. Multi-Conf. Eng., Educ., and Technol.*, Boca Raton, FL, USA, Jul. 2022, doi: 10.18687/LACCEI2022.1.1.508.